Journal of Molecular Structure 1319 (2025) 139506

Contents lists available at ScienceDirect

Journal of Molecular Structure

journal homepage: www.elsevier.com/locate/molstr

Synthesis and structural elucidation of cytotoxic mono and dinuclear rhenium carbonyl complexes bearing bis-{1,3-(imino pyrrolyl)-*m*-chloro phenyl)} ligand

Diksha [a], Maharaja Somasundaram [c], Mathan Ganeshan [c], Satish Kumar Samal [d], Dhanasekaran Dharumadurai [e], Sherzod Madrahimov [f], Akshi Deshwal [a], Harminder Kaur [a,*], Alessandro Sinopoli [b,*], Veeranna Yempally [f,*]

[a] *Chemistry Department, Punjab Engineering College, Chandigarh 160012, India*
[b] *Qatar Environment and Energy Research Institute (QEERI), Hamad Bin Khalifa University, Doha, Qatar*
[c] *Department of Biomedical Science, Bharathidasan University, Tiruchirappalli, Tamil Nadu 620024, India*
[d] *Institute of Nano Science and Technology, Sector-81, Knowledge City, Mohali, Punjab 140306, India*
[e] *Department of Microbiology, Bharathidasan University Tiruchirappalli, Tamil Nadu 620 024, India*
[f] *Division of Arts&Sciences, Texas A&M University at Qatar, Doha, Qatar*

ARTICLE INFO

Keywords:
Imino pyrrolyl ligands
Rhenium (I) complexes
DFT
Anticancer
IC_{50} values

ABSTRACT

A mononuclear and dinuclear rhenium tricarbonyl compounds were synthesized by the one-pot condensation reaction of [*Re*$(CO)_5$Br], pyrrole-2-carboxaldehyde and 4-chloro-*m*-phenylene diamine. The mononuclear rhenium tricarbonyl complex containing {3-(imino pyrrolyl)-6-chloro phenylamine)} ligand (IPP) with formula {[*Re*$(CO)_3$Br(IPP)], (**1**), was obtained by refluxing stoichiometric quantities of amine, aldehyde and rhenium metal precursor in methanol solution. Similarly, dinuclear rhenium tricarbonyl compound {[*Re*$(CO)_3$Br]$_2$(BIPP)], BIPP = bis-{1,3-(imino pyrrolyl)-*m*-chlorophenyl)}, (**2**) has been synthesized by refluxing appropriate amounts of aldehyde, and rhenium metal precursor in the presence of one equivalent of amine ligand. Compounds **1** and **2** were characterized by FT-IR, ^{1}H NMR, and UV–Vis spectroscopy, elemental analysis, and mass spectrometry. The luminescence properties of the formed complexes were studied in solution at room temperature, revealing an extended lifetime for the dinuclear complex **2** in comparison to **1**. DFT calculations for the optimized structures helped to understand the geometry of the complexes, whereas TD-DFT revealed the vertical transitions responsible for the photophysical properties of the complexes. The cytotoxicity of such complexes against MCF-7 breast cancer has been also reported, revealing a dose-dependent growth inhibition attributed to a DNA-intercalating mode of binding for both complexes. The pronounced effect of the two metals on the cytotoxic studies and lifetime of the excited species were investigated. The greater intercalation ability of the complex **2** in comparison to complex**1** obtained from circular dichroism studies also indicates the greater efficacy of *Re* complex 2.

1. Introduction

The rampant growth of cancer is one of the leading causes of death worldwide which has led to the development of several therapeutic approaches including radiation therapy, chemotherapy, immuno-therapy, etc. [1]. The success of cisplatin and other platinum-based drugs has paved the way for the employment of metal complexes as potent agents for chemotherapy [2]. However, the lack of selectivity and the severe side effects associated with platinum-based anticancer agents limited their use and necessitated the discovery of new anticancer scaffolds with greater specificity and selectivity [3,4]. In this regard, organometallic Rhenium complexes are arising as potential alternatives to platinum-based anticancer agents [5,6]. Rhenium and technetium carbonyl complexes with various chelating bidentate ligands have been explored recently as potential candidates in the development of radio-pharmaceuticals and imaging applications [7]. The past decade has seen a rapid rise in the design and development of novel (*Re*$(CO)_3$) complexes for exploration of their anti-proliferative activity [8]. Researchers have

* Corresponding authors.
E-mail addresses: hkaur@pec.edu.in (H. Kaur), asinopoli@hbku.edu.qa (A. Sinopoli), vyempally@gmail.com (V. Yempally).

https://doi.org/10.1016/j.molstruc.2024.139506
Received 15 April 2024; Received in revised form 16 July 2024; Accepted 29 July 2024
Available online 30 July 2024
0022-2860/© 2024 Elsevier B.V. All rights are reserved, including those for text and data mining, AI training, and similar technologies.

exploited the facile coordination capacity of ancillary ligands to the biological molecule of interest (tumor cells, estrogen receptors) and the kinetic inertness of these complexes due to the presence of strong-field ligands for developing new anti-proliferative drugs containing rhenium carbonyl complexes [9,10]. The stable fac-$[Re(CO)_3]^+$ core is well suited for the synthesis of hexacoordinate *fac*-rhenium carbonyl complexes with a variety of chelating ligands possessing unique features such as high photostability, long emission lifetimes, and large stokes shifts which makes them attractive candidates for biological imaging [11]. Rhenium tricarbonyl complexes with diimine ligands such as phenanthroline, bipyridine can also be employed for fluorescent cellular imaging owing to the presence of accessible long-lived triplet metal-to-ligand charge transfer (^{3}MLCT) states [12,13]. These salient features afford additional advantage over the traditional platinum based complexes as they can be explored for the theranostic applications [11, 14].

The plethora of research in this field is now aiming at incorporating selective functional groups on the backbone of chelating ligands to enhance permeability into the tumor cells, selective binding to the specific target, and improving their solubility in the aqueous medium [15]. Heteroaromatic compounds, such as pyrrole and indole, are predominantly present in several natural products and also in several biologically active molecules possessing excellent pharmacological activities and antiproliferative properties [16]. There are only a few coordination complexes of rhenium (MRP-20) with pyrrole derivatives reported in the literature regarding application in radiopharmaceuticals and anti-cancer drugs [17,18]. Moreover, there are only a handful of pyrrolyl imine ligands coordinated rhenium carbonyl complexes reported in the literature [18–21], as shown in Scheme 1.

The biological activity of such *Re* (I) complexes can be tuned by varying the structural properties of the diimine ligand while retaining their photophysical properties [22–24]. The binding of *Re*(I) carbonyl complexes containing pyrrolyl imine ligands to biological molecules of interest (MOI) can be controlled by decorating the ligand with selective functional groups such as hydroxyl, amine, or aldehyde [25]. Another strategy adopted to enhance cellular uptake and cytotoxicity is by incorporating halogen substituents either in the primary coordination sphere or the secondary coordination sphere. The beneficial effect of Cl and F atoms in enhancing the biological potency of several drugs is well established, and recently similar research findings have pointed to the remarkable increase in the cytotoxicity and cell penetration selectively to tumor cells[26]. The success of several monometallic complexes has inspired researchers to develop novel strategies to combine various metal centers in one compound, to create a heterobimetallic complex that could integrate the diverse modes of action that are typical of the constituent metal centers [27–29]. The corresponding treatment strategy should require less concentration of the drug due to the combining of multiple activities into a single molecule while reducing the side effects associated with high dosages of less effective drugs. This will be translated in a lower IC50 value or in overcoming issues associated with resistance to the available treatments. The conjunction of $(Re(CO)_3)$ core with other metal centers, to obtain bimetallic complexes, has led to the synergistic effect between the two metals [30]. This synergistic effect often leads to enhanced cytotoxicity and improved biological activity, as reported by several studies [31]. Furthermore, *Re*(I) complexes with diimine ligands have found applications in fluorescent bioimaging [32, 33].

In the current work, our main target is to synthesize novel rhenium carbonyl complexes with pyrrolylimine ligands, decorated with heteroatom substituents, for investigating their photoluminescence and biological activity. We report the synthesis of mono and dinuclear rhenium (I) tricarbonyl $(Re(CO)_3)$ complexes bearing iminopyrrolyl ligand by one-pot condensation method involving aromatic diamines and pyrrole-2-carboxaldehyde (pyca). The synthesized $(Re(CO)_3)$ complexes were fully characterized with the help of FT-IR, ^{1}H NMR, UV–visible spectroscopy, and DFT calculations. The *in vitro* cytotoxic activities of the synthesized *Re* complexes against human breast cancer cell line MCF-7 were evaluated. The experimental investigation pointed out that the addition of a second metal center, in the dinuclear complex, induced a pronounced effect on the cytotoxicity and increased the lifetime of excited species. DNA binding studies, including absorption titrations and circular dichroism, indicated that both complexes bind to DNA through an intercalative mode.

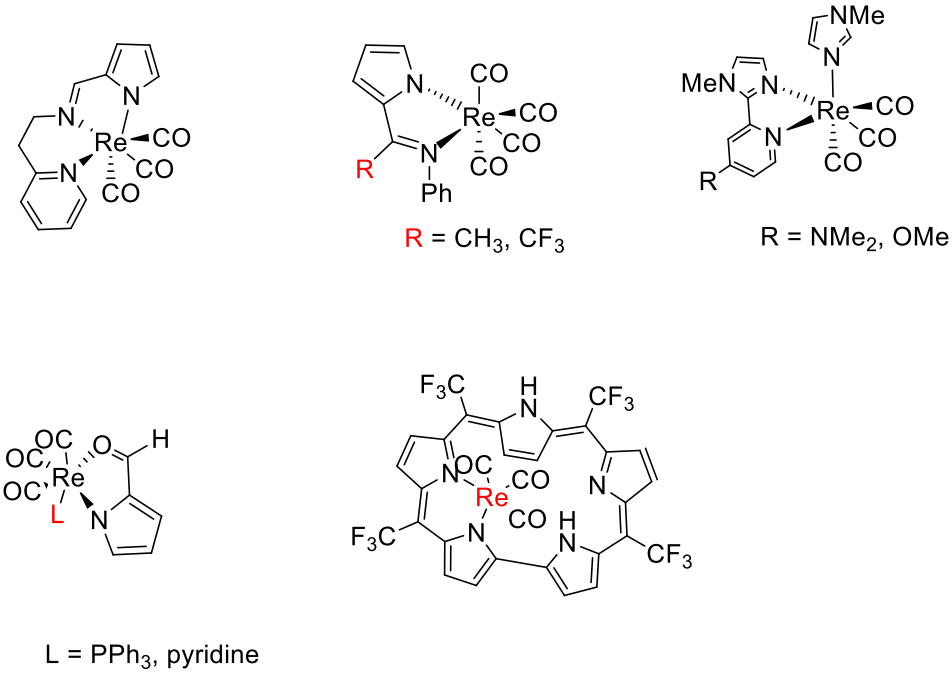

Scheme 1. Main rhenium pyrrolyl imine carbonyl complexes reported so in literature [18–21].

2. Experimental section

2.1. Materials and methods

All chemicals and solvents used were purchased from Sigma-Aldrich and used as received without further purification. Infrared Spectra of formed metal complexes were recorded with a Perkin Elmer Spectrum Two spectrometer. NMR Spectra was recorded on Bruker Avanche II 400NMR Spectrometer. Absorption spectra were recorded on Systronics Double Beam Spectrophotometer 2203 using DMF and DMSO as solvents. Circular dichroism (CD) measurements were carried out using a Biologic spectrophotometer (Science Instruments) with a 1 mm pathlength quartz cell. The concentration of CT-DNA used for the CD measurement was 50 μg/mL and 1 mM for metal ions in a 5 mM Tris-HCl (pH=7) buffer.

2.2. Computational calculations

The ground state geometries and electronic structures of (*Re*$(CO)_3$(IPP)Br)) **(1)** and (*Re*$(CO)_3$Br(BIPP)*Re*$(CO)_3$Br) **(2)** were calculated according to density functional theory (DFT) calculations using the GAUSSIAN-09 software package (Gaussian, Inc.)[34]. The computational investigation has been done using the LANL2DZ basis set for the *Re* atom and 6–311+*G*(d,p) basis set for other atoms like C, H, N, O, Cl, and Br[35], to obtain the molecular geometry optimization, vibrational frequencies, and vertical transitions at the DFT/B3LYP level for the *Re* complexes in the ground state.

2.3. Cytotoxic studies

Human breast cancer cell line MCF-7 was obtained from the National Centre for Cell Science, Pune, India. Cells were grown in Dulbecco's Modified Eagle Medium (DMEM) high glucose media containing 10 % Fetal Bovine Serum (FBS), Antibiotic, and Antimitotic solution (Hi Media, India). Cells were incubated at 37 °C humidified chamber at 5 % CO_2 condition. Cell viability was determined using MTT (3-(4, 5-Dimethylthiazol-2-yl)−2, 5-Diphenyltetrazolium Bromide). MCF-7 breast cancer cells are planted at $5{\cdot}10^3$ cells/well in 96 well plates for 24 h. Following that, cells were treated with varying concentrations of the two metallic complexes. Each metallic complex was removed after 24 h of incubation and replaced with 30 μl of MTT reagent (0.5 mg/mL). After 4 h of incubation at 37 °C, the MTT solution was removed, and the Formazan crystals were dissolved in DMSO (200 mL/well). After that, the plate was read at 570 nm. The obtained data was visually represented as percent viability vs. concentrations, and the IC50 was calculated. For the apoptosis analysis, the cells were plated in a 6-well plate and treated with the two different metallic complexes. The treated and untreated cells were incubated with acridine orange and ethidium bromide solution and examined under a fluorescent microscope. The percentage of apoptosis cell death is then calculated.

2.4. Synthesis of IPP

The ligand IPP was synthesized by stirring pyrrole-2-carboxaldehyde (1 mmol) and 4-chloro-*m*-phenylene diamine (1 mmol) in dry $CH_2C\ l_2$ for 24 h. The reaction mixture was concentrated on a rotary evaporator, washed with hexane, and dried to obtain IPP. (70 % yield)

^{1}H-NMR data ($CDCl_3$, ppm): δ 8.19 (s, 1H), 7.21–7.20 (m, 1H), 6.92 (s, 1H), 6.67–6.66 (m, 1H), 6.58 (s,1H), 6.54–6.52 (m,1H), 6.29–6.28 (m, 1H). IR (KBr, cm^{-1}): (NH stretch) 3438, 3290, 3217 cm^{-1} (CN stretch) 1597 cm^{-1}, HRMS-ESI (*m/z*): 220.0650.

2.5. Synthesis of BIPP

The BIPP ligand was synthesized according to the procedures already reported in the literature but with slight modification. 2 equivalents of pyrrole-2-carboxaldehyde and 1 equivalent of 4-chloro-*m*-phenylene diamine were mixed in absolute ethanol in the presence of catalytic amount of *p*-toluenesulfonic acid (ptsa). The mixture was refluxed overnight and all the volatiles were removed and washed with dichloromethane to obtain the corresponding BIPP ligand.

^{1}H-NMR data ($CDCl_3$, ppm): δ 9.5 (s, 1H), 8.19 (s, 1H), 7.87 (s, 1H), 7.26–6.1 (aromatic H), IR (KBr, cm^{-1}): (NH stretch) 3238 cm^{-1}, (CN stretch) 1627 cm^{-1}. HRMS-ESI (*m/z*): 297.1110.

2.6. Synthesis of [Re(CO)$_3$(IPP)Br] (1)

4-chloro-*m*-phenylene diamine (1 mmol) was mixed with pyrrole-2-carboxaldehyde (1 mmol) in methanol for 20 min. [*Re*$(CO)_5$Br] (1 mmol) was added and the mixture was refluxed for **4 h**. Compound 1 was obtained by slow evaporation of the solvent, washed with hexane and diethyl ether, and dried. (Scheme 3)

Yield (80 %), IR (KBr, cm^{-1}): (CO stretch) 2020, 1886 cm^{-1}, UV/Vis (DMSO): λ_{max} (ε, $M^{-1}cm^{-1}$) = 267 nm, 322 nm. ^{1}H-NMR data (DMSO-d_6, ppm): δ 8.3 (s, 1H), 7.30–7.25 (m, 1H), 7.24–7.21 (m, 1H), 6.74–6.71 (m, 1H),6.3–6.2 (m,1H), 5.8–5.2 (bs,2H).

Elemental analysis $C_{14}H_{12}BrClN_3O_3Re$ (569.81); calc. C 29.41; H 2.12; N 7.35; Meas. C 29.81, H 2.10, N 7.41. HRMS-ESI (*m/z*): 569.8772

2.7. Synthesis of [Re(CO)$_3$Br(BIPP)Re(CO)$_3$Br] (2)

The bimetallic compound was prepared by the one-pot condensation method [4,*Re*$(CO)_5$Br]. (2 mmol), 4-chloro-*m*-phenylene diamine (1 mmol), and pyrrole-2-carboxaldehyde (2 mmol) were refluxed in methanol for 4 h resulting in a violet color solution. The solvent was evaporated slowly on a rotary evaporator to obtain compound **2**, followed by washing with hexane and diethyl ether. **(**Scheme 3**)** Yield (85 %)

IR (KBr, cm^{-1}): (CO stretch) 2016, 1893, UV/Vis (DMSO): λ_{max} (ε, M–1cm–1) = 281 nm, 577.5 nm. ^{1}H-NMR data (DMSO-d_6, ppm): δ 7.95 (s, 2H), 7.30–7.26 (m, 1H), 7.26–7.23 (m, 2H), 7.18–7.16 (m, 2H), 7.15–7.13(m, 1H), 6.74–6.73(s, 1H). Elemental analysis $C_{22}H_{13}Br_2ClN_4O_6Re_2$ (997.04); calc C 26.50; H 1.31; N 5.62; Meas. C 27.0, H 1.59, N 5.59. HRMS-ESI (*m/z*): 996.7579

3. Results and discussion

The general interest in developing new rhenium carbonyl complexes for theranostic applications has motivated us to design two new pyrrolylimine ligands IPP and BIPP, with desired functionalities appropriate for enhancing the cytotoxicity of the corresponding complexes. As shown in Scheme 2, the ligand IPP is characterized by a bidentate moiety, with nitrogen from the pyrrole and one from the imine fragments, together with a halogen Cl and an amine substituent to facilitate coordination to biological MOI. Similarly, the ligand BIPP also possesses a Cl substituent, an extended conjugation to enhance absorption in visible light, and two bidentate moieties to accommodate two metal centers. We explored the effect of two metal centers and heteroatoms on the biological activity of the metal complexes [*Re*$(CO)_3$(IPP)Br] **(1)**, and [*Re*$(CO)_3$Br(BIPP)*Re*$(CO)_3$Br] **(2)**, specifically in their anti-cancer activity. The synthesis of phenylene bridged dinuclear *Re*(I) complex **(2)** and mononuclear *Re*(I) complex **(1)** by one-pot condensation method is here reported. These two *Re* complexes (**1** and **2**) were easily synthesized by the reaction of *Re*$(CO)_5$Br, phenylene diamines, and pyrrole-2-carboxaldehyde in appropriate stoichiometries as shown in Scheme 3. The one-pot reaction of [*Re*$(CO)_5$Br], pyrrole-2-carboxaldehyde, and phenylene diamine produced metal-bound Schiff base complexes in good yields(80–85 %). The reaction proceeded through the initial formation of a yellow solution of Schiff base and subsequently the change of color to red indicates the formation of metal complexes.

Both compounds **1** and **2** are air-stable in a solid state for several months. Compound **1** is completely soluble in polar solvents like

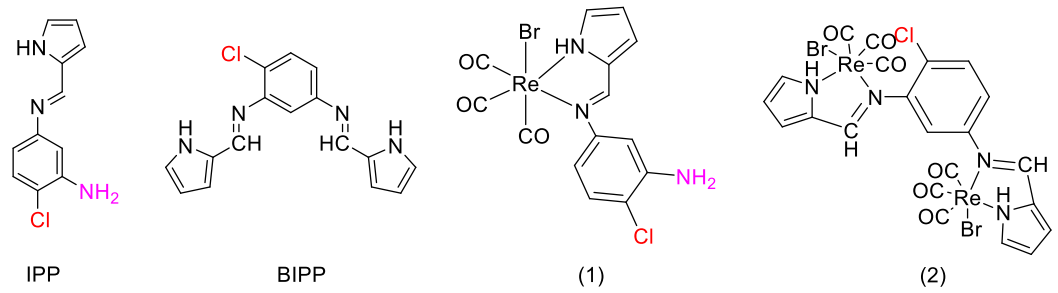

Scheme 2. Ligands and rhenium carbonyl complexes are reported in this work.

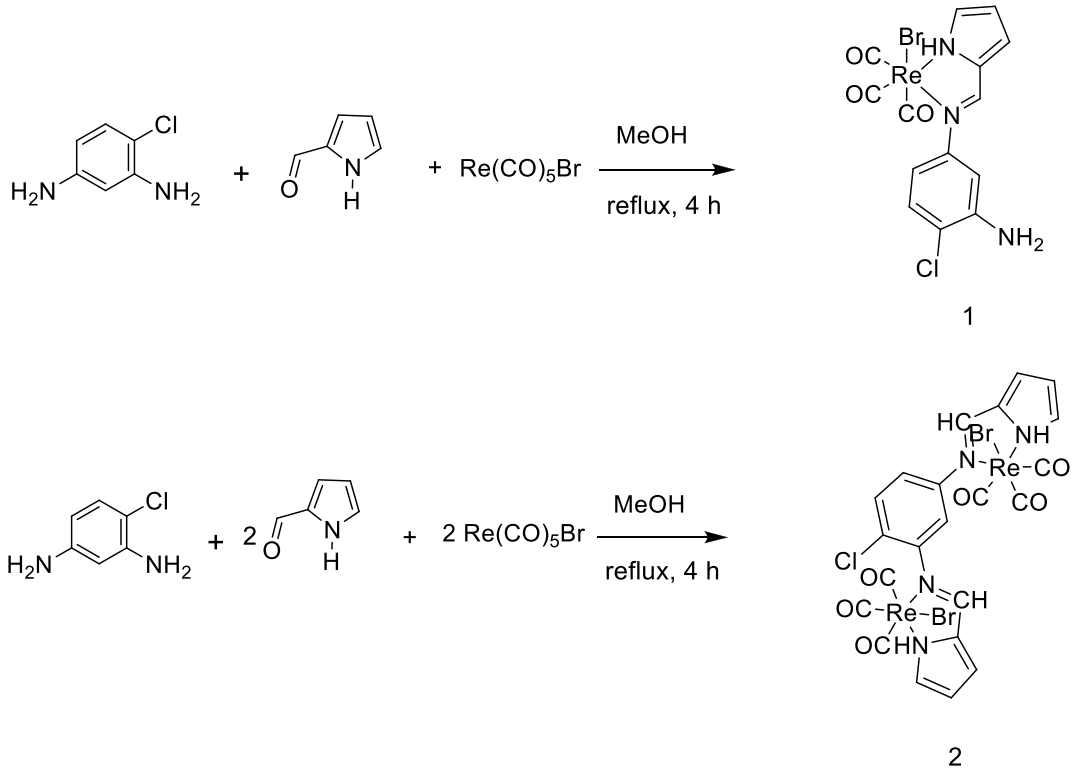

Scheme 3. One pot synthesis of Rhenium carbonyl complexes 1 (top), and 2 (bottom).

acetonitrile and methanol, and sparingly soluble in dichloromethane. Compound **2** has limited solubility in methanol and acetonitrile, but is highly soluble in DMSO and DMF. Both compounds are stable in air even in a solution state for several weeks without decomposition. Unfortunately, several attempts to isolate suitable crystals of **1** and **2** for single-crystal XRD studies were unsuccessful even after several attempts. However, structural elucidation of compounds **1** and **2** was completed with the help of FT-IR, DFT, and ^{1}H NMR spectroscopic techniques. The synthesized *Re* complexes were fully characterized by UV-visible spectroscopy, photoluminescence, and TGA to prove the thermal stability of **1** and **2**. The ESI-mass spectra of both compounds also match with the assigned structures of the rhenium carbonyl complexes.

HRMS of the synthesized ligands IPP, BIPP, and their corresponding rhenium complexes **1** and **2** are shown in supplementary data. The molecular ion peak for the ligands IPP, and BIPP was observed at *m/z* 220.06, and 297.09 corresponding to the M+1 peak respectively, confirming the formation of the ligands IPP and BIPP. The high-resolution mass spectrum of mononuclear *Re* (I) complex **[*Re*(CO)$_3$(IPP)Br] (1)**, contains the molecular ion peak and other fragmentation peaks were also obtained by successive loss of CO ligands, -Br ligand, etc. The molecular ion peak for **1** was obtained at *m/z* 570, and the loss of the bromine ligand gave a peak in the mass spectra at 490. Further, the loss of carbonyl ligands occurs successively and peaks were obtained at *m/z* 462, 434, and 406. Whereas the dinuclear *Re* (I) complex **[*Re*(CO)$_3$Br (BIPP)*Re*(CO)$_3$Br] (2)** shows the molecular ion peak at *m/z* 998.9.

The synthesis of compounds **1** and **2** by two-step synthesis with the use of monomer ligands IPP and dimer ligand BIPP was also attempted to compare and identify any new intermediate species in the two-step reaction [36]. The ligands IPP and BIPP were synthesized separately in pure form and they were used in stoichiometric proportion in the reaction with rhenium pentacarbonyl bromide in the toluene solution to yield compounds **1** and **2** respectively. No other intermediate species or new products were observed. However, the isolated yields from one pot synthesis were higher compared to the two-step process as described earlier. The Schematic representation of the synthesis of complexes **1**, and **2** using two-step procedures is summarised in Scheme 4.

The rhenium carbonyl complexes **1** and **2** have facial geometry as confirmed by both carbonyl stretching frequencies in the region observed for similar *fac*-rhenium carbonyl complexes [37,38]. Unlike other reported rhenium carbonyl complexes with pyrrolyl imine ligands, compounds **1** and **2** both retain the proton on the pyrrolic nitrogen atom and halide bromine atom coordinated to rhenium metal in the axial position. The ^{1}H-NMR spectra of both **1** and **2** in DMSO-d$_6$ have distinct peaks at around 9.0 to 9.5 ppm corresponding to the imine hydrogen

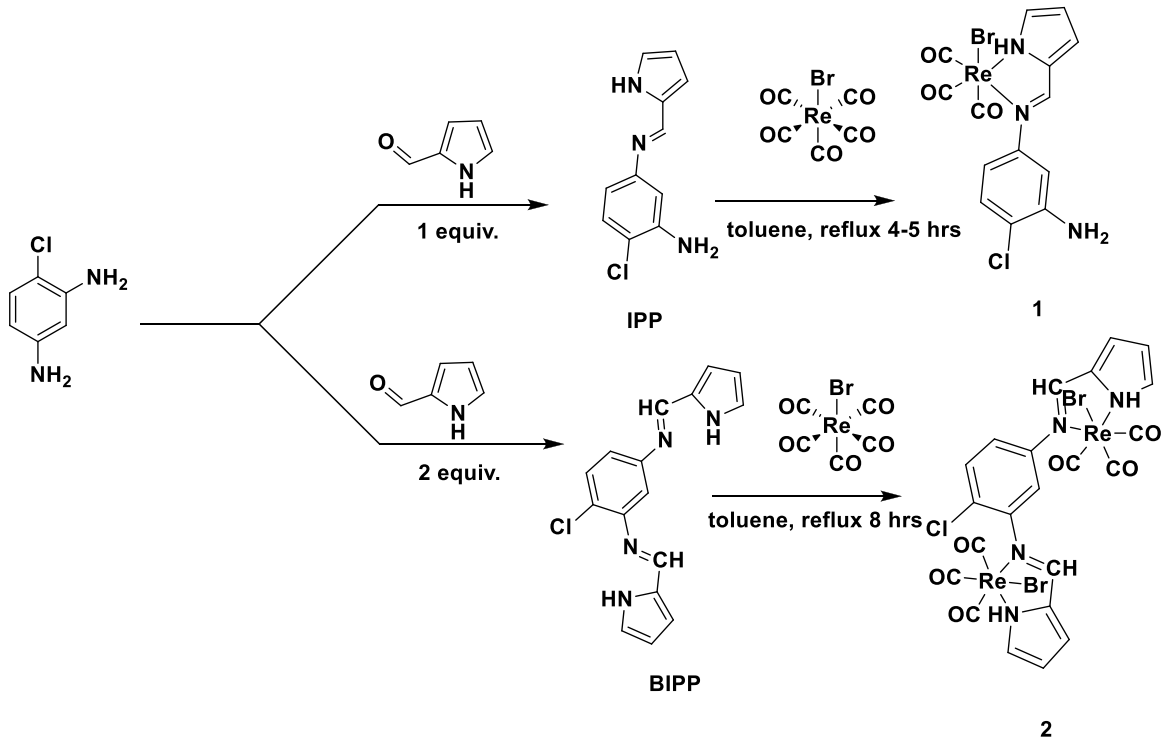

Scheme 4. Synthesis protocol for rhenium carbonyl complexes 1 and 2.

atom which appears in the deshielded region [39]). The ^{1}H NMR of **1** and **2** are shown in Figs S14 and S15. The ^{1}H NMR of both the ligands IPP and BIPP is recorded in $CDCl_3$. For the ligand IPP, the peak at δ 10 ppm corresponds to –NH proton of the pyrrole ring [39]. The free –NH2 groups show peak at around 4 ppm. The imine proton shows peak at around 8.1 ppm. The aromatic protons of the phenyl ring were observed at around 7 ppm with the protons of the pyrrole ring were slightly shielded and obtained at around 6 ppm. Similarly, for the ligand BIPP, the imine proton shows sharp peak at δ 8.25 ppm. The characteristic peak in the synthesized complexes **1** and **2** are the imine proton peaks obtained at around 9.5 ppm and are shifted downfield compared to imine protons in the ligands. The aromatic protons are obtained as multiplet in the range 6.9–8 ppm.

The complex **2** showed limited solubility in most solvents. In addition to this, the presence of the bromine on the same and opposite sides of the phenylenediimine plane leads to isomerization and is also responsible for the complex nmr spectra. The elemental analysis shows the experimentally observed elemental analysis data matches with the calculated data.

3.1. Vibrational properties

The FT-IR spectra of ligands IPP and BIPP contain azomethine linkage i.e. ν (C=N) groups in the range 1580–1630 cm^{-1} as shown in Figs. S3 and S4. The significant elongation of the *Re*-Br bond in **1** and **2**, compared to the similarly reported compound [*Re*$(CO)_3$(bpy)Br] (*Re*-Br 2.58 Å), with bond length of 2.638 and 2.640 Å in **1** and **2** respectively, suggests increased donation of electron density from the diimine ligands IPP and BIPP to rhenium metal, and reducing the donation of σ electron density from the bromide ligand making its release more facile [40]. The mononuclear complex **1** and dinuclear complex **2** have markedly different IR spectra. The observed carbonyl stretching frequency values are slightly higher for mononuclear complex **1** (2029, 1892 cm^{-1}) than the corresponding dinuclear rhenium complex **2** (2012, 1883 cm^{-1}) which is associated with the enhanced π back bonding in dinuclear complexes. The stretching vibrational frequencies of 1 and 2 are listed in Table 1 [41–43]. The FT-IR spectra of the synthesized *Re* complexes **1** and **2,** match well with the already reported facial-rhenium tricarbonyl complexes showing three CO stretching frequencies [44,45] with the two lower energy CO bands sometimes merged into a single broad band [41]. The synthesized *Re* carbonyl complexes contain only two carbonyl stretching vibrational bands showing the merging of the two closely spaced CO bands.

To better understand the vibrational frequencies of the reported molecules, we performed DFT frequency calculations on the synthesized *Re* complexes **1** and **2** using the B3LYP model and LANL2DZ basis set [46,47]. A scale factor of 0.9679 is introduced to account for the basis set deficiencies and electron correlation effects in the calculations. The experimentally and theoretically observed FT-IR spectra for complexes **1** and **2** are shown in supplementary data. The theoretically obtained FT-IR contains three CO stretching peaks (2095, 1976, and 1920) for complex 1, whereas the experimental spectra show the merging of two lower energy CO bands. Similarly, the C=N stretching frequencies were obtained experimentally at 1597 cm^{-1} and theoretically at 1634 cm^{-1}. Upon taking into consideration scaling factor, the theoretical CO stretching frequencies were reduced to 2027, 1912, 1858 cm^{-1}). Similarly, the C=N stretching frequency became 1581 cm^{-1} upon introduction of scaling factor to account for the basis set deficiencies. The theoretical vibrational frequencies matches well with the experimentally obtained values. The scenario is more articulated for the dinuclear rhenium complex **2** due to the presence of a large number of possible distinct vibrational modes for the dinuclear complexes [41].

3.2. Photophysical properties

UV-visible absorption spectra of complexes were recorded in DMSO. Typically, UV-visible absorption spectra of *Re*$(CO)_3$ diimine complexes show two types of electronic transitions [5]. The first absorption band below 300 nm can arise result from π→π* transitions. Instead, the weaker bands at lower energy are assigned to singlet metal to ligand charge transfer MLCT bands [48], characterized by low absorptivity due to their spin-forbidden nature. The lower energy charge transfer band

arising due to the $t_2g \rightarrow \pi^*$ transition is sensitive to the nature of the solvent. More polar solvents shift the band to higher energy. The mononuclear complex *Re*$(CO)_3$(pyca-pH)Br shows two strong absorption peaks at 262, 319 nm assigned as Ligand Centered (LC) $\pi \rightarrow \pi^*$ transition. Whereas the main transition in dinuclear complex **2** lies at 261 nm and peaks arising due to metal to ligand charge transfer at 526 nm as shown in Fig. 1. In comparison to the mononuclear complex, the dinuclear complex exhibits more intense MLCT absorption band.

The mononuclear and dinuclear complexes **1** and **2**, upon photoexcitation at different wavelengths, i.e., 271, 332, 402, 455 and 464 nm, displayed broad and featureless emission in the visible region of light, characterized by two bands at 498 and other at ~650 nm, as shown in Fig. 2. The emission features are independent of the excitation energy and similar spectra are observed for tricarbonyl-*Re* based complexes [35]. The emission intensity resulted higher for Complex **2** than for Complex **1** when excited with higher energy (271, 332, 402 nm), whereas the trend is just opposite when excited with low energy light (455, 464 nm). The excitation spectra of both the complexes corresponding to the 498, 650 nm emissions are shown in Fig. 3 and they consist of four bands at 271, 332, 402, and 455 nm. These band positions are in accordance with the absorbance spectra of these complexes. However, the intensity is different because the non-radiative decay of the excited state plays a crucial role in the intensity of the excitation bands. The emission profile for rhenium tricarbonyl species generally consists of a single broad band due to the transition from the lowest ^{3}MLCT excited state to the ground state, generally associated with a relatively short lifetime in the ns range [49].

The lifetime analysis of excited species for **1** and **2** after excitation at 455 nm was investigated in DMSO solvent at 498 and 650 nm emissions. The decay plots for both compounds **1** and **2** for 498 emissions follow the single exponential decay pathway with the excited state lifetime values of 3.7 and 4.2 ns, respectively as shown in Fig. 4. However, the 650 nm emission decays biexponentially for both the complexes. The shorter lived component (τ_2) due to decay of LLCT excited state (π-π^*), and (τ_1) component is assigned to decay of MLCT state. The assignments of transitions arising from excited state were investigated in detail using the TD-DFT calculations and will be discussed in detail in the computational calculations section. A similar biexponential decay pathway was also observed for the compound [*Re*$(CO)_3$((n-N)(btpz)], where bptz = 3,5-bis(trifluoromethyl) pyrazolate[50]. The emission lifetime of the mononuclear complex *Re*$(CO)_3$(IPP)Br (**1**) is found to be shorter than the emission lifetime of the dinuclear complex *Re*$(CO)_3$Br(BIPP)*Re*$(CO)_3$Br (**2**) (Fig. 4). The electronic properties of the synthesized *Re* complexes are summarized in Table 2.

3.3. Theoretical calculations on Re(I) complexes

The GAUSSIAN 09 software package[51] with B3LYP functional is employed for optimizing the geometries of mononuclear and dinuclear *Re* complexes **1** and **2** respectively with LANL2DZ basis set [46] for the *Re* atom and 6–311+*G*(d,p) basis set [46] for other atoms like C, H, N, Cl, Br and O. As per the DFT calculations, the optimized ground state geometry exhibited by (*Re*$(CO)_3$(IPP)Br)) (**1**) and (*Re*$(CO)_3$Br(BIPP)*Re*$(CO)_3$Br) (**2**) is distorted octahedral around the rhenium metal center. In both *Re* complexes, rhenium metal is coordinated to nitrogen of the imine group of the Schiff base and nitrogen of the pyrrole ring. The three carbonyl ligands are coordinated to *Re* (I) facially and the sixth coordination site is occupied by the bromine ligand. The equatorial position is occupied by the other two carbonyl groups and two nitrogen atoms of the ligand **IPP** and **BIPP** in **1** and **2** respectively. The *Re* –CO bond lengths are found in the range 1.90–1.92 Å, these bond lengths obtained are consistent with the reported rhenium carbonyl complexes [52].

The DFT-optimized structures of *Re* complex **1** and **2** are shown in (Fig. 5).

Among the electronic properties, the energies of the HOMO and LUMO orbitals are very important in quantum chemistry. The highest occupied molecular orbital (HOMO is mainly localized on the metal centre. The HOMO of both **1** and **2** exhibits mixed contribution from dπ (*Re*), pπ(Br), and π orbitals of carbonyl groups, whereas the LUMO has more π^* character corresponding to π^* orbital of Schiff base ligand as shown in Fig. 6. The HOMO-LUMO analysis further reveals the transfer of electron density from ligand to metal which further suggests that the possible transitions are LMCT charge transfer transitions. The stability of the synthesized *Re* complexes **1** and **2** was evaluated by finding various chemical reactivity parameters such as electronegativity (χ), ionization potential (IP), electron affinity (EA), hardness (η), chemical potential (μ), and electrophilicity index (ω) etc. as listed in Table 3. The chemical reactivity parameters were obtained from the energy of HOMO and LUMO orbitals. The energy difference between the highest occupied molecular orbital (HOMO) and the lowest unoccupied molecular orbital (LUMO) also known as energy gap (Eg) determines the stability and reactivity of the compounds. The lower energy gap of complex 2 (2.99 eV) in comparison to **1** (2.99 eV) suggests the greater reactivity of complex **2**. The synthesized *Re* complexes show higher ionization

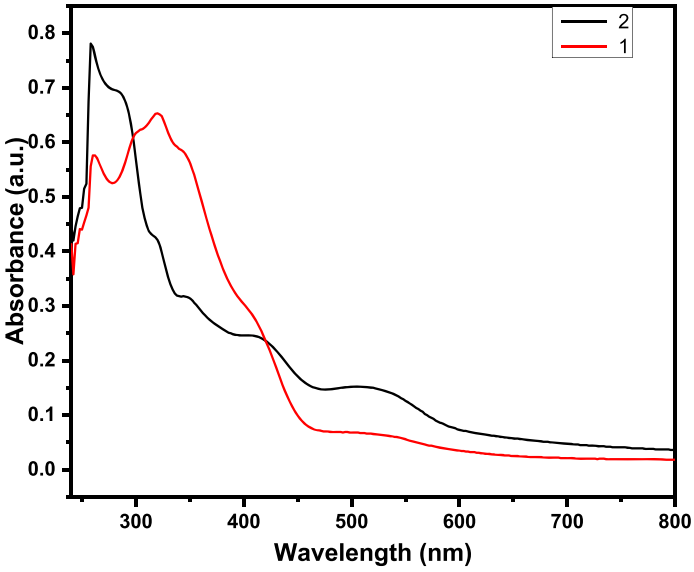

Fig. 1. UV-visible absorption spectra of formed complexes in DMSO at room temperature.

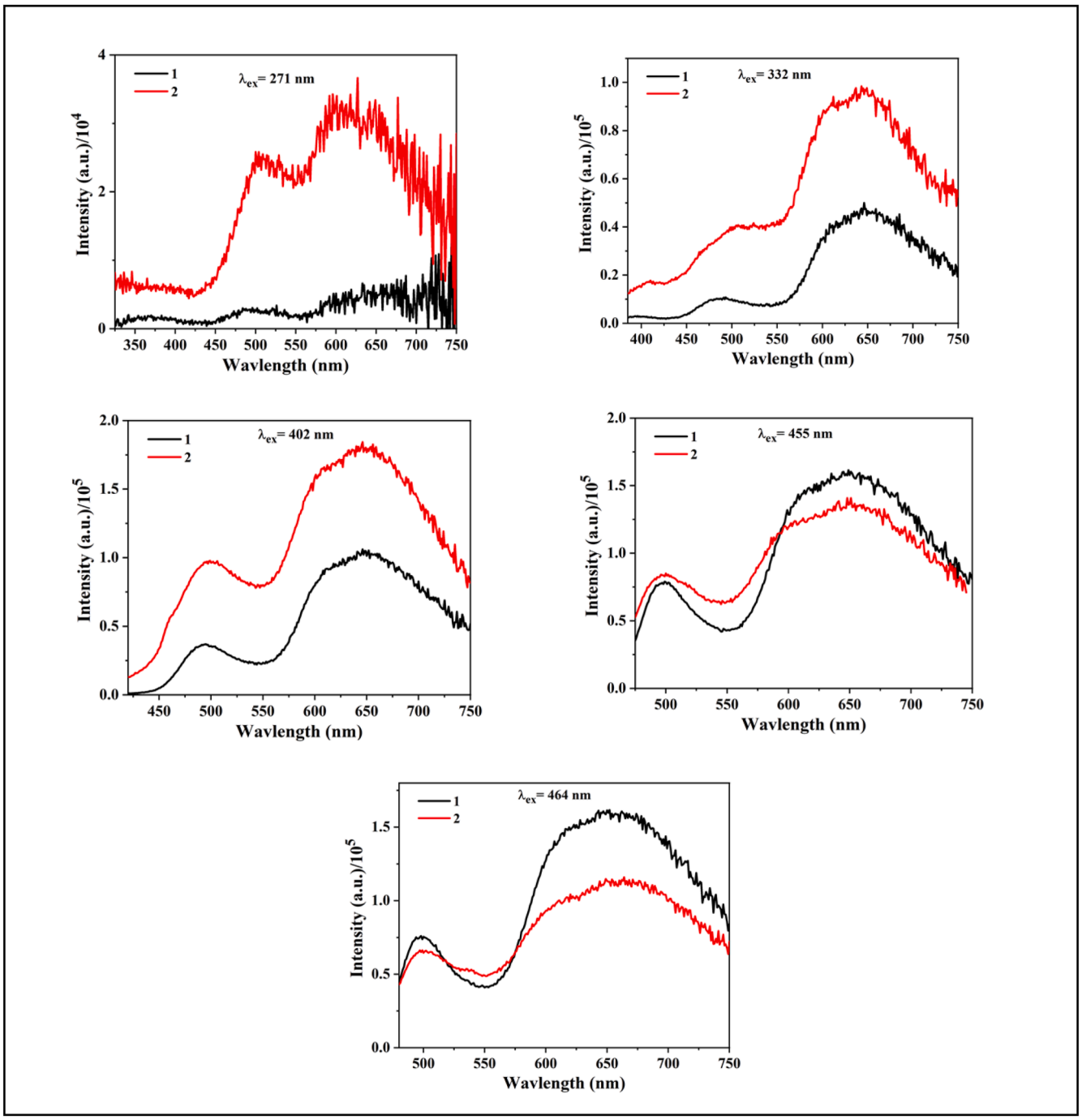

Fig. 2. Emission spectra of *Re* complex **1** and **2** at different excitation wavelengths.

potential values than the electron affinity values indicating the greater electron donation ability of the complexes than the electron accepting power. The compound **2** has higher electronegativity and electrophilicity index than **1** as shown in Table 3 which further suggests the greater ability of compound **2** to interact with a biological target by means of covalent bond or H-bonding. The findings of global reactivity parameters provide evidence regarding the acceptance and donor ability, hardness, chemical reactivity of the synthesized complexes which is related to the biological activities.

3.4. Cytotoxic studies of the synthesized re complexes (1 and 2) against MCF-7 breast cancer cell line

The cytotoxic activity of the synthesized rhenium carbonyl complexes has been explored against the MCF-7, the breast cancer cell line (Fig. 7). The results obtained indicate that **1** and **2** inhibit MCF-7 cells in a dose-dependent manner. MCF-7 cells were inhibited by exposure to complex **2**, with an IC50 of 40 μM. **1** inhibited breast cancer cell growth at 75 μM. The higher efficacy of **2** in comparison to **1** against the MCF-7 breast cancer line was attributed to the possible synergistic effect of 2 rhenium centers in **2**. Also, the cellular uptake and cytotoxicity are largely affected by lipophilicity and molecular size of the compound [53]. The presence of a halogen atom on the aromatic ring enhances the

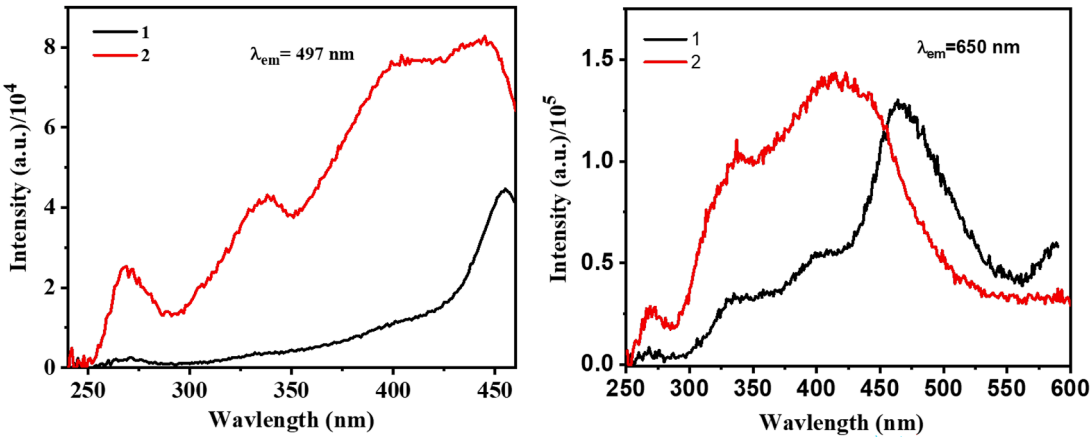

Fig. 3. Excitation spectra of *Re* complex **1** and **2** at different emission wavelengths.

Table 1
Selected vibrational frequencies in (cm^{-1}) for the *Re* complexes **1** and **2**.

Complex	νCO [cm^{-1}]		νC═N [cm^{-1}]
	A_1	E	
***Re*(CO)$_3$(IPP)Br (1)**	2029	1892	1597
***Re*(CO)$_3$Br(BIPP)*Re*(CO)$_3$Br (2)**	2012	1883	1627

Table 2
Electronic spectral data of *Re* complexes (**1, 2**) at room temperature.

Complex	UV visible absorption/nm			
	LC	MLCT	λ_{em}	τ/ns
***Re*(CO)$_3$(pyca-pH)Br**	262, 319	530	498, 650	3.7,6.7
***Re*(CO)$_3$Br(*m*-PPC)*Re*(CO)$_3$Br**	261	526	498, 650	4.2, 9.5

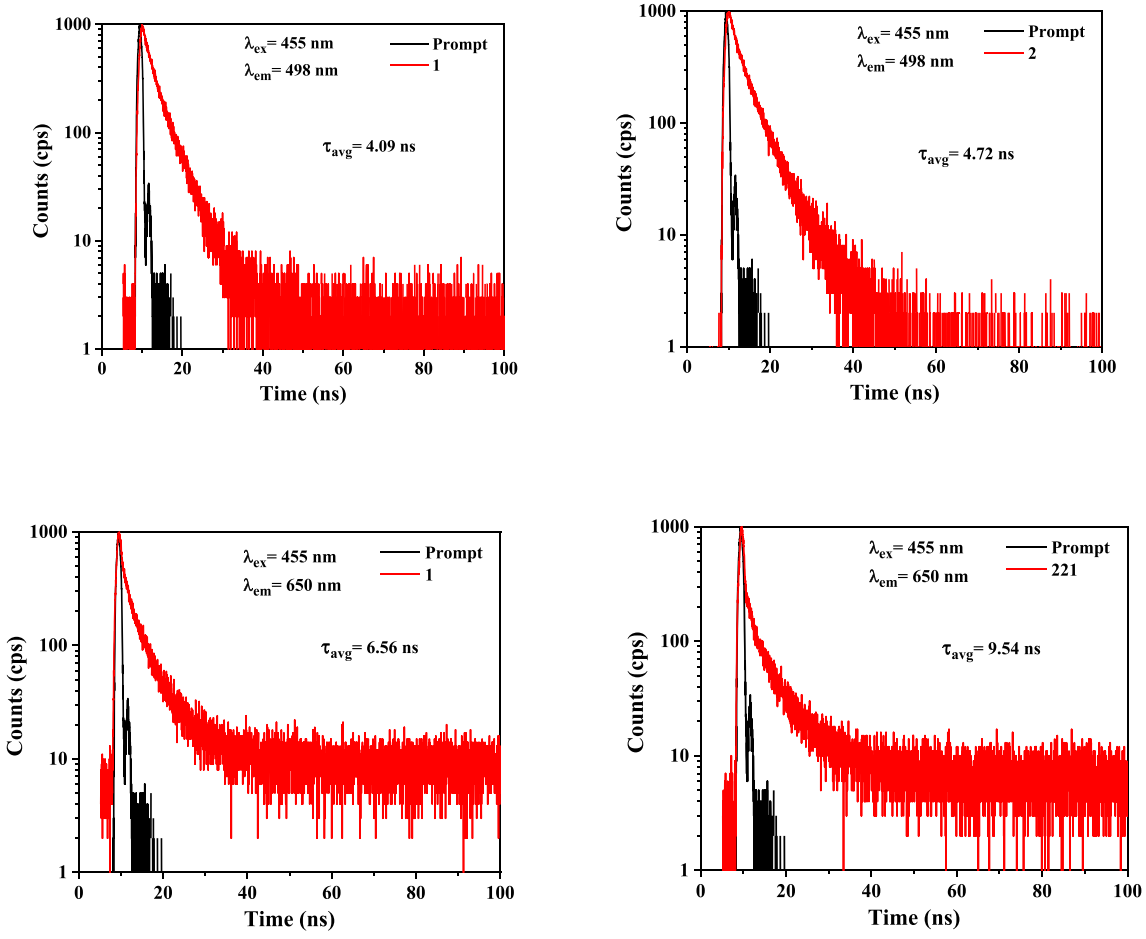

Fig. 4. Photoluminescence lifetime decay measurements of *Re* complex **2** (top right), *Re* complex **1**(top left) recorded at 498 nm corresponding to the 1st emission peak, and lifetime decay measurements of *Re* complex **2** (bottom right), *Re* complex **1**(bottom left) recorded at 650 nm corresponding to the 2nd emission peak.

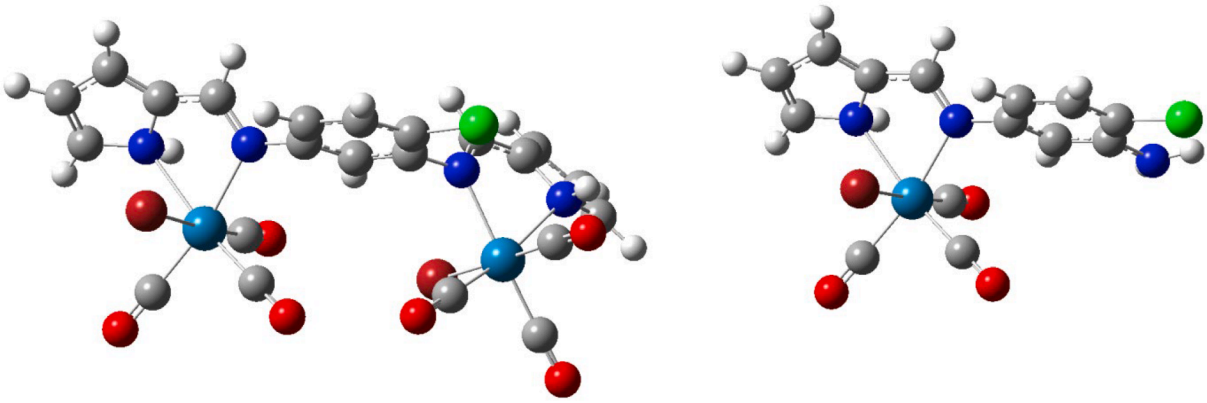

Fig. 5. Optimised geometry of **2**(left), and **1** (right). Color code: red for O, blue for N, gray for C, white for H, green for Cl, dark red for Br, steel blue for *Re*.

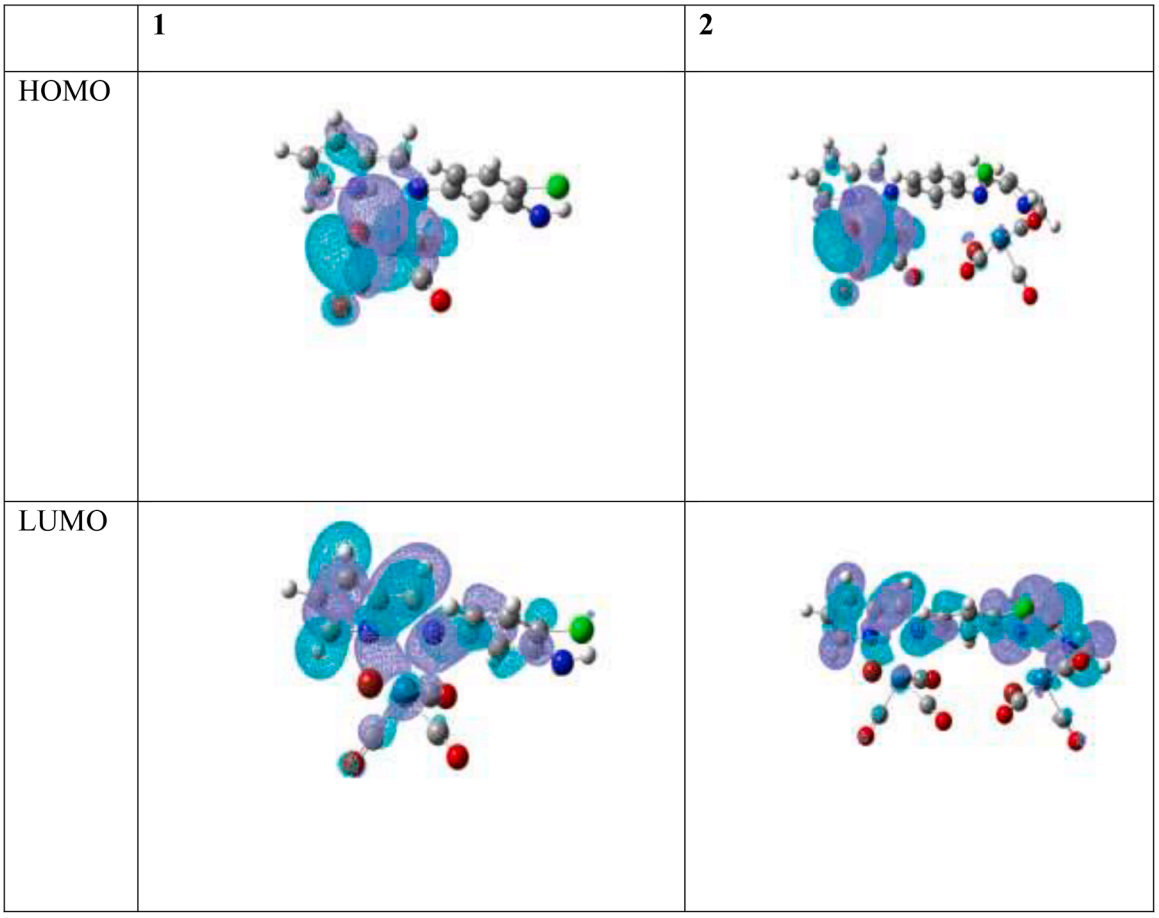

Fig. 6. Molecular orbital surfaces for **1** and **2**, HOMO (top) and LUMO (bottom).

Table 3
Calculated Global reactivity descriptor parameters of **1** and **2**.

Global reactivity descriptors	1	2
E_{HOMO} (eV)	−6.07	−6.07
E_{LUMO} (eV)	−2.91	−3.08
ΔE (LUMO-HOMO) (eV)	3.16	2.99
Chemical hardness (η)	1.58	1.49
Ionization potential (IP)	6.07	6.07
Electron affinity (EA)	2.91	3.08
Electronegativity (χ)	4.49	4.57
Chemical potential (μ)	−4.49	−4.57
Electrophilicity index (ω)	6.37	6.94

lipophilicity which increases the ability of the molecule to interact with various cancer lines [54]. Further, the greater cytotoxicity of dinuclear rhenium complex **2** might be due to the possible synergistic effect and greater lipophilicity of the rhenium complex **2** in comparison to mononuclear rhenium complex **1**. Ye et al. have also observed increased lipophilicity of bidentate ligands in dinuclear rhenium complexes and found that the dinuclear complexes possess improved anticancer efficacy than the mononuclear counterparts [53].

3.5. *Apoptotic nuclear morphology assessment*

Cells that have been treated with the two organometallic complexes

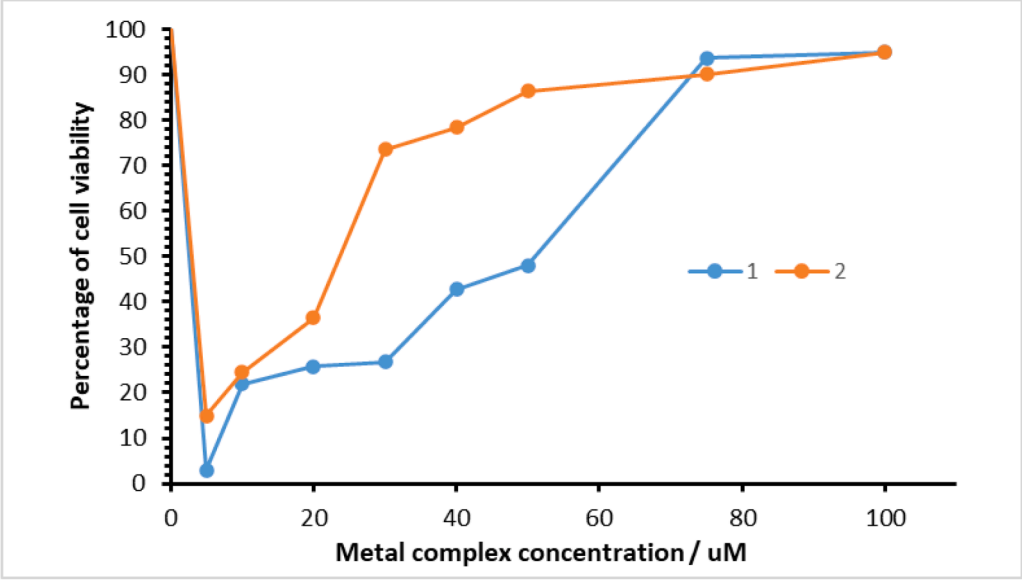

Fig. 7. Breast cancer growth inhibition by complex **1** and **2**. Data shown are mean ± SD. *$p < 0.05$, compared with respective control (untreated cells).

are subject to different biological changes, that accompany apoptotic cell death, including cell shrinkage, nuclear condensation, DNA breakage, blebbing, and the creation of apoptotic bodies. The chromatin condensation in the stained nucleus was confirmed by the results of the AO/EB staining, which also helped to distinguish between viable, apoptotic, and necrotic cells (Fig. 8). The apoptotic cells had uniform bright orange nuclei. The nuclei of the viable cells were uniformly green. Cancer cells treated with compounds **1** and **2** showed signs of apoptosis, such as altered cell size and nuclear fragmentation, when stained with AO/EB. Compounds **1** and **2**′s anticancer activity may result from the induction of apoptosis against MCF-7. The fluorescence pattern of the stain is determined by the vitality and membrane integrity of the cells in this staining approach. Live cells are exclusively permeable to acridine orange and so glow green, but dead cells are permeable to ethidium bromide and fluoresce orange-red. After the complex was treated, all of these morphological alterations were found.

3.6. DNA binding studies

The calf-thymus (CT-DNA) was prepared in 5 mM Tris–HCl buffer solution (pH= 7.4) and stored at 4 °C. The CT-DNA was adequately free of protein contamination as indicated by the UV absorption ratio of 1.86 at 260 and 280 nm. The interaction between the synthesized metal complexes **1** and **2** with the DNA was carried out by performing the absorption titrations at fixed concentrations of metal complexes while varying the concentration of CT-DNA.

UV-visible absorption spectroscopy is one of the simplest methods to study the binding affinity between the CT-DNA and the synthesized complexes. The change in the electronic absorption spectra upon the gradual addition of CT-DNA is shown in Fig. 9. It was observed that the addition of CT-DNA leads to a decrease in the absorbance value of the complexes leading to a hypochromic effect. The significant hypochromic shift suggests intercalative mode of binding,

3.7. Circular dichroism

CD spectroscopic technique has been successfully employed to determine the conformational changes induced by the interaction of DNA with the metal complex. The CD spectra of CT-DNA were recorded over a scan range of 220–360 nm and it has been found to contain one positive band at 275 nm arising due to base stacking and one negative band at 247 nm due to helicity [55]. The minor groove binding mode of interaction showed only a little perturbation on the base stacking and helicity bands while the intercalative binding mode caused enhancement in the intensities of both the bands. Incubation of DNA with complexes **1** and **2** leads to enhancement of the intensity of both the positive and negative bands with no considerable shift in λ_{max} observed (Fig. 10). These changes observed support the intercalative mode of binding [56]. Furthermore, large spectral band changes were observed in dinuclear rhenium complex **2** in comparison to mononuclear rhenium

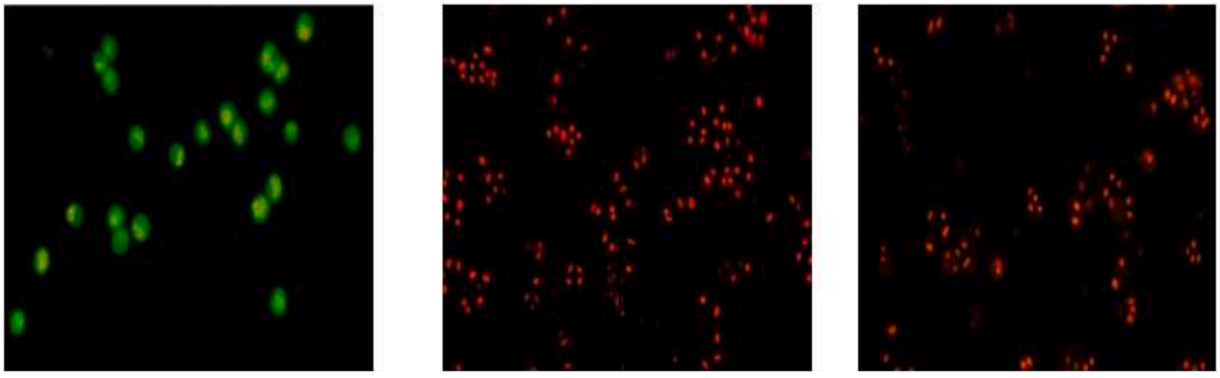

Fig. 8. Apoptotic nuclear morphology assessment, control (left), complex **1** (middle), complex **2** (right).

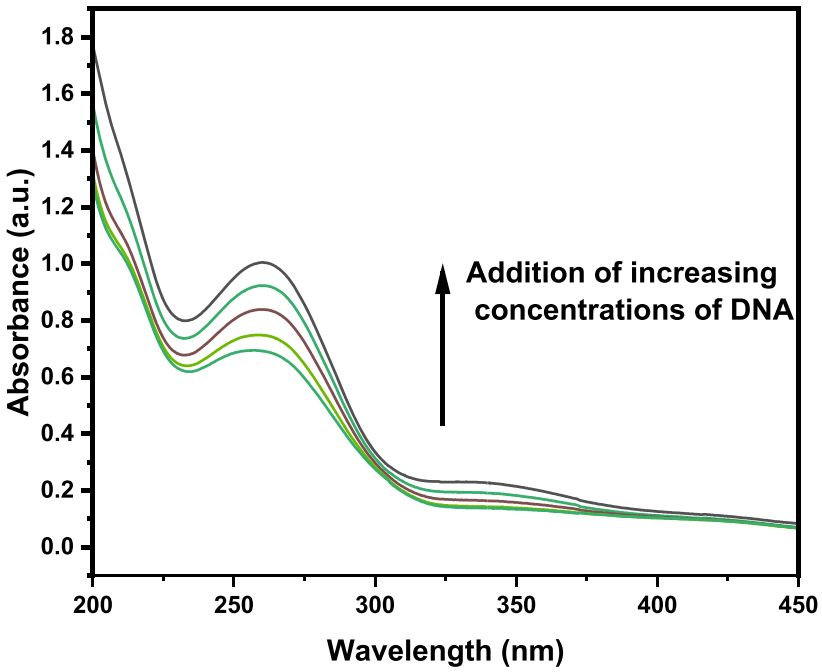

Fig. 9. Absorption spectra of complex **2** (1 mM) in 5 mM Tris–HCl/50 mM NaCl buffer upon addition of increasing amounts of DNA.

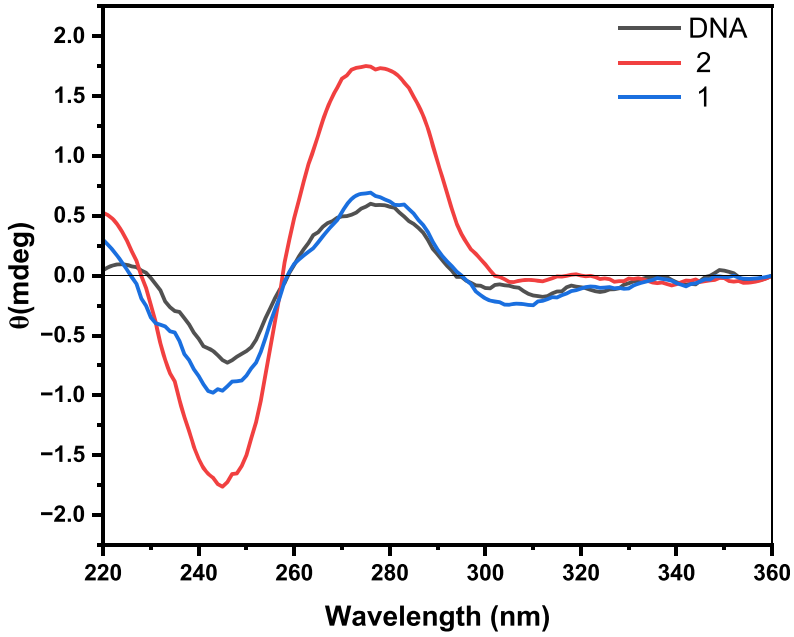

Fig. 10. CD spectra of CT-DNA, and the interaction with complexes (**1** and **2**). All the spectra were recorded in 5 mM Tris–HCl/50 mM NaCl buffer, pH 7.2 and 25 °C.

complex **1** suggesting the greater intercalation ability of complex **2** [55].

4. Conclusion

Two new rhenium carbonyl complexes with iminopyrrolyl ligands were synthesized, characterized and their photophysical properties were studied. The cytotoxic activity of the synthesized rhenium complexes was evaluated against breast cancer cell line MCF-7. The rhenium complexes **1** and **2** induce cell death by apoptosis causing damage to mitochondria, nucleus, and intracellular generation of reactive oxygen species (ROS). Complexes **1** and **2** interact with cellular DNA via intercalative binding mode as evidenced by DNA binding studies and circular dichroism. The dinuclear rhenium complex **2** inhibits breast cancer cell growth at 40 μM while the IC50 value of mononuclear rhenium complex **1** is 75 μM. The greater efficacy of rhenium carbonyl complex **2** in comparison to **1** could be due to the possible synergistic effect of **2** rhenium centers in complex **2**. This is further supported by the CD studies which suggest the greater intercalation ability of complex **2**. The findings contribute valuable insights into the design and application of rhenium carbonyl complexes in cancer therapy.

Funding

The authors declare that no funds or grants were received during the preparation of this manuscript.

Ethics approval

Not Applicable.

Consent to participate

Informed consent was obtained from all the authors involved.

Consent to publish

The authors have consented to the submission of research work to the Journal of Molecular Structure.

CRediT authorship contribution statement

Diksha: Writing – review & editing, Writing – original draft, Investigation, Formal analysis, Data curation. **Maharaja Somasundaram:** Formal analysis. **Mathan Ganeshan:** Data curation. **Satish Kumar Samal:** Data curation. **Dhanasekaran Dharumadurai:** Formal analysis. **Sherzod Madrahimov:** Data curation. **Akshi Deshwal:** Data curation. **Harminder Kaur:** Supervision, Resources. **Alessandro Sinopoli:** Investigation, Formal analysis, Data curation. **Veeranna Yempally:** Writing – review & editing, Supervision, Methodology, Conceptualization.

Declaration of competing interest

The authors declare that they have no known competing financial interests or personal relationships that could have appeared to influence the work reported in this paper.

Data availability

Data will be made available on request.

Acknowledgements

Diksha would like to acknowledge Punjab Engineering College (PEC) and MHRD for providing GATE fellowship.We would like to thank Science & Engineering Research Board (SERB) (File.No: EEQ/2018/001446 Dated 22 March 2019) for providing their project funding and student fellowship.

Supplementary materials

Supplementary material associated with this article can be found, in the online version, at doi:10.1016/j.molstruc.2024.139506.

References

[1] B.K. Singh, Spectroscopic, electrochemical and biological studies of the metal complexes of the Schiff base derived from pyrrole-2-carbaldehyde and ethylenediamine, Arab. J. Chem. (2012), https://doi.org/10.1016/j.arabjc.2012.10.007.
[2] C. Ko, G. Li, C. Leung, D. Ma, Dual function luminescent transition metal complexes for cancer theranostics : the combination of diagnosis and therapy, Coord. Chem. Rev. 381 (2019) 79–103, https://doi.org/10.1016/j.ccr.2018.11.013.
[3] Z. Huang, J.J. Wilson, Therapeutic and diagnostic applications of multimetallic rhenium (I)tricarbonyl complexes, Eur. J. Inorg. Chem. (2021) 1312–1324, https://doi.org/10.1002/ejic.202100031.
[4] A. Hasheminasab, H.M. Rhoda, L.A. Crandall, J.T. Ayers, V.N. Nemykin, R. S. Herrick, C.J. Ziegler, Hydrazine-mediated strongly coupled *Re*(CO)3 dimers, Dalton Trans. 44 (2015) 17268–17277, https://doi.org/10.1039/c5dt02821c.
[5] I. Maisuls, E. Wolcan, O.E. Piro, E.E. Castellano, G. Petroselli, R. Erra-Balsells, F. M. Cabrerizo, G.T. Ruiz, Synthesis, structural characterization and biological evaluation of rhenium(I) tricarbonyl complexes with β-carboline ligands, ChemistrySelect 2 (2017) 8666–8672, https://doi.org/10.1002/slct.201701961.
[6] L.D. Ramos, H.M. Da Cruz, K.P. Morelli Frin, Photophysical properties of rhenium (i) complexes and photosensitized generation of singlet oxygen, Photochem. Photobiol. Sci. 16 (2017) 459–466, https://doi.org/10.1039/c6pp00364h.
[7] G.V. Sidorenko, A.E. Miroslavov, Higher technetium (i) carbonyls and possibility of using them in nuclear medicine : problems and prospects, Radiochemistry 63 (2021) 253–262, https://doi.org/10.1134/S1066362221030012.
[8] A. Sharma S, V. Nee, B. Kar, U. Das, P. Paira, Target-specific mononuclear and binuclear rhenium(I) tricarbonyl complexes as upcoming anticancer drugs, RSC Adv. 12 (2022) 20264–20295, https://doi.org/10.1039/d2ra03434d.
[9] A. Leonidova, G. Gasser, Underestimated potential of organometallic rhenium complexes as anticancer agents, ACS Chem. Biol. (2014) 2180–2193.
[10] Influence of the substituent on the phosphine ligand in novel rhenium(I) aldehydes. Synthesis, computational studies and first insights into the antiproliferative activity, Dalton Trans. (2018) 13861–13869, https://doi.org/10.1039/c8dt03160f.
[11] K. Ranasinghe, S. Handunnetti, I.C. Perera, T. Perera, Synthesis and characterization of novel rhenium (I) complexes towards potential biological imaging applications, Chem. Cent. J. (2016) 1–10, https://doi.org/10.1186/s13065-016-0218-4.
[12] L.K. Mckenzie, H.E. Bryant, J.A. Weinstein, Transition metal complexes as photosensitisers in one- and two-photon photodynamic therapy, Coord. Chem. Rev. 379 (2019) 2–29, https://doi.org/10.1016/j.ccr.2018.03.020.
[13] T.M. Mclean, J.L. Moody, M.R. Waterland, S.G. Telfer, Luminescent rhenium(I)-dipyrrinato complexes, Inorg. Chem. 51 (2012) 446–455, https://doi.org/10.1021/ic201877t.
[14] C.C. Konkankit, S.C. Marker, K.M. Knopf, J.J. Wilson, Anticancer activity of complexes of the third row transition metals, rhenium, osmium, and iridium, Dalton Trans. (2018) 9934–9974, https://doi.org/10.1039/c8dt01858h.
[15] M.N. Pinto, P.K. Mascharak, Light-assisted and remote delivery of carbon monoxide to malignant cells and tissues: photochemotherapy in the spotlight, J. Photochem. Photobiol. C Photochem. Rev. 42 (2020) 100341.
[16] Computational design of rhenium(I) carbonyl complexes for anticancer photodynamic therapy, Inorg. Chem. 61 (2022) 439–455, https://doi.org/10.1021/acs.inorgchem.1c03130.
[17] F. Morgan, R. Thornback, Rhenium(V) and technetium(V) complexes with N-[2 (1H-pyrolylmethyl)]-N′-(4-pentene-3-one-2) ethane-1,2-diaminate (C12H16N3O, MRP 20). X-ray crystal structures of H3MRP 20 and TcO(MRP 20), Inorg. Chim. Acta (1991) 257–264.
[18] P. Yadav, N. Fridman, A. Mizrahi, Z. Gross, Rhenium(i) sapphyrins: remarkable difference between the C6F5 and CF3-substituted derivatives, Chem. Commun. 56 (2020) 980–983, https://doi.org/10.1039/c9cc08877f.
[19] J. Mirebeau, F.Le Bideau, Synthesis of Rhenium Carbonyl Complexes Bearing Substituted Pyrrolyl Ligands, Organometallics 27 (2008) 2911–2914.
[20] C.Y. Chan, P.A. Pellegrini, I. Greguric, P.J. Barnard, Rhenium and technetium tricarbonyl complexes of N-heterocyclic carbene ligands, Inorg. Chem. 53 (2014) 10862–10873, https://doi.org/10.1021/ic500917s.
[21] A. Shegani, C. Triantis, C. Kiritsis, C. Raptopoulou, V. Psycharis, M. Pelecanou, I. Pirmettis, M. Papadopoulos, Neutral fac-[*Re*(NNN)(CO)3] complexes with NNN tridentate ligands containing pyrrole or indole, Inorg. Chem. Commun. 63 (2016) 1–4, https://doi.org/10.1016/j.inoche.2015.11.002.
[22] C.C. Konkankit, B.A. Vaughn, S.N. Macmillan, E. Boros, J.J. Wilson, Combinatorial synthesis to identify a potent, necrosis-inducing rhenium anticancer agent, Inorg. Chem. (2019), https://doi.org/10.1021/acs.inorgchem.8b03552.
[23] S. İrişli, S. Günnaz, Ö. Özcan, A. Arı, M. Maral, A. Erdem, D. Özel, F. Yurt, Platinum (II) schiff base complexes and their effects on the inhibition of amyloid β1–42 aggregation, Appl. Organomet. Chem. (2024) 1–16, https://doi.org/10.1002/aoc.7540.
[24] A.E.M. Abdallah, S.A. Abdel-Latif, G.H. Elgemeie, Novel fluorescent benzothiazolyl-coumarin hybrids as anti-SARS-COVID-2 agents supported by molecular docking studies: design, synthesis, X-ray crystal structures, DFT, and TD-DFT/PCM calculations, ACS Omega 8 (2023) 19587–19602, https://doi.org/10.1021/acsomega.3c01085.
[25] S. Muhammad, V. Yempally, M. Anas, S. Moncho, S.J. Kyran, E.N. Brothers, D. J. Darensbourg, A.A. Bengali, Mechanism of CO displacement from an unusually labile rhenium complex: an experimental and theoretical investigation, Inorg. Chem. (2012) 13041–13049.
[26] D. Chiodi, Y. Ishihara, Magic Chloro ": profound effects of the chlorine atom in drug discovery, J. Med.Chem. 66 (2023) 5305–5331.
[27] Z. Pan, L. He, Dinuclear phosphorescent rhenium(i) complexes as potential anticancer and photodynamic therapy agents, Dalton Trans. 49 (2020) 11583–11590, https://doi.org/10.1039/d0dt02424d.
[28] E.B. Bauer, A.A. Haase, R.M. Reich, D.C. Crans, F.E. Kühn, Organometallic and coordination rhenium compounds and their potential in cancer therapy, Coord. Chem. Rev. 393 (2019) 79–117, https://doi.org/10.1016/j.ccr.2019.04.014.
[29] E. Giorgi, F. Binacchi, C. Marotta, A. Pratesi, D. Cirri, C. Gabbiani, Highlights of new strategies to increase the efficacy of transition metal complexes for cancer treatments, Molecules 28 (2023) 273.
[30] V. Fern, M. Concepci, Heterobimetallic complexes for theranostic applications, Chem. Eur. J. 24 (2018) 3345–3353, https://doi.org/10.1002/chem.201705335.
[31] C.B. Smith, L.C. Days, D.R. Alajroush, K. Faye, Y. Khodour, S.J. Beebe, A.A. Holder, Special issue invited review photodynamic therapy of inorganic complexes for the treatment of cancer, Photochem. Photobiol. (2022) 17–41, https://doi.org/10.1111/php.13467.
[32] C.C. Konkankit, E. Boros, Combinatorial synthesis to identify a potent, necrosis-inducing rhenium anticancer agent, Inorg. Chem. 58 (2019) 3895–3909, https://doi.org/10.1021/acs.inorgchem.8b03552.

[33] K. Schindler, F. Zobi, Photochemistry of rhenium (I) diimine tricarbonyl complexes in biological applications, Chimia 75 (2021) 837–844, https://doi.org/10.2533/chimia.2021.837 (Aarau).
[34] M. Caricato, M.J. Frisch, A. Frisch, J. Hiscocks, M.J. Frisch, Gaussian 09 IOps reference manual, 2013. http://www.gaussian.com/g_tech/g_iops/iops2.pdf.
[35] A. Comia, L. Charalambou, S.A.E. Omar, P.A. Scattergood, P.I.P. Elliott, A. Sinopoli, Photophysical and electrocatalytic properties of rhenium(I) triazole-based complexes, Inorganics 8 (2020) 1–13, https://doi.org/10.3390/inorganics8030022.
[36] A.I. Adebomi, A.O. Abimbola, O.E. Gabriel, Synthesis, physicochemical and antimicrobial properties of rhenium (I) tricarbonyl complexes of isatin Schiff bases, African J. Biotechnol. 20 (2021) 175–185, https://doi.org/10.5897/ajb2020.17291.
[37] D. Vitale, Facial rhenium tricarbonyl complexes with modified DII ligands facial rhenium tricarbonyl complexes with modified DII ligands, Inorg. Chem. Commons (2019).
[38] R. Kia, S. Mahmoudi, P.R. Raithby, New rhenium-tricarbonyl complexes bearing halogen-substituted bidentate ligands structural, computational and Hirshfeld surfaces studies, CrystEngComm 21 (2019) 77–93, https://doi.org/10.1039/c8ce01860j.
[39] A. Charles, R. Krishnaveni, K. Sivaraj, Synthesis, characterization of metal complexes of schiff base derived from pyrrole-2-carbaldehyde and 4-methoxy aniline and their biological studies, Asian J. Chem. 32 (2020) 3012–3018.
[40] T. Auvray, A.K. Pal, G.S. Hanan, Electronic properties of rhenium(I) carbonyl complexes bearing strongly donating hexahydro-pyrimidopyrimidine based ligands, Eur. J. Inorg. Chem. 2021 (2021) 2570–2577, https://doi.org/10.1002/ejic.202100028.
[41] R. Jordan, M. Niazi, S. Schäfer, W. Kaim, A. Klein, Rhenium tricarbonyl complexes of azodicarboxylate ligands, Molecules 27 (2022), https://doi.org/10.3390/molecules27238159.
[42] S. Frantz, M. Sieger, I. Hartenbach, F. Lissner, T. Schleid, J. Fiedler, C. Duboc, W. Kaim, Structure, electrochemistry, spectroscopy, and magnetic resonance, including high-field EPR, of {(μ-abpy)[*Re*(CO)3X]2}o/•-, where abpy = 2,2′-azobispyridine and X = F, Cl, Br, I, J. Organomet. Chem. 694 (2009) 1122–1133, https://doi.org/10.1016/j.jorganchem.2008.09.034.
[43] W. Kaim, S. Kohlmann, The nature of reduced and excited states of π-electron-deficient complexes between *Re*(CO)3Hal and diimine ligands, Inorg. Chem. 29 (1990) 2909–2914, https://doi.org/10.1021/ic00341a010.
[44] S. Frantz, J. Fiedler, I. Hartenbach, T. Schleid, W. Kaim, A complete series of tricarbonylhalidorhenium(I) complexes (abpy)*Re*(CO)3(Hal), Hal = F, Cl, Br, I; abpy = 2,2′-azobispyridine: structures, spectroelectrochemistry and EPR of reduced forms, J. Organomet. Chem. 689 (2004) 3031–3039, https://doi.org/10.1016/j.jorganchem.2004.06.047.
[45] H. Hartmann, T. Scheiring, J. Fiedler, W. Kaim, Structures and spectroelectrochemistry (UV-vis, IR, EPR) of complexes [(OC)3ClRe]n(abpy), n = 1, 2; abpy = 2,2′-azobispyridine, J. Organomet. Chem. 604 (2000) 267–272, https://doi.org/10.1016/S0022-328X(00)00282-5.
[46] D. Álvarez, M.I. Menéndez, R. López, Computational design of rhenium(I) carbonyl complexes for anticancer photodynamic therapy, Inorg. Chem. 61 (2022) 439–455, https://doi.org/10.1021/acs.inorgchem.1c03130.
[47] K. Choroba, A. Maroń, A. Świtlicka, A. Szłapa-Kula, M. Siwy, J. Grzelak, S. Maćkowski, T. Pedzinski, E. Schab-Balcerzak, B. Machura, Carbazole effect on ground- and excited-state properties of rhenium(i) carbonyl complexes with extendedterpy-like ligands, Dalton Trans. 50 (2021) 3943–3958, https://doi.org/10.1039/d0dt04340k.
[48] K.K. Lo, J.S. Lau, V.W. Fong, Properties of a luminescent rhenium (I) polypyridine anthraquinone complex with a thiourea receptor, Mercury (2004) 1098–1106.
[49] H. Xia, X. Liu, Synthesis, structure, and luminescence of rhenium (I) complexes with substituted bipyridines, J. Coord. Chem. (2012) 37–41, https://doi.org/10.1080/00958972.2012.671479.
[50] A. Coleman, C. Brennan, J.G. Vos, M.T. Pryce, Photophysical properties and applications of *Re*(I) and *Re*(I)-Ru(II) carbonyl polypyridyl complexes, Coord. Chem. Rev. 252 (2008) 2585–2595, https://doi.org/10.1016/j.ccr.2008.07.001.
[51] L.O. Ahmed, R.A. Omer, Journal of physical chemistry and functional materials population analysis and UV–Vis spectra of dopamine molecule using gaussian 09, J. Phys. Chem. Funct. Mater. 3 (2020) 48–58. https://dergipark.org.tr/jphcfum.
[52] J.F. Martinez, N.T. La Porte, S. Chaudhuri, A. Sinopoli, Y.J. Bae, M. Sohail, V. S. Batista, M.R. Wasielewski, Effect of electronic coupling on electron transfer rates from photoexcited naphthalenediimide radical anion to *Re*(bpy)(CO)3X, J. Phys. Chem. C 123 (2019) 10178–10190, https://doi.org/10.1021/acs.jpcc.8b12264.
[53] R.R. Ye, C.P. Tan, M.H. Chen, L. Hao, L.N. Ji, Z.W. Mao, Mono- and dinuclear phosphorescent rhenium(I) complexes: impact of subcellular localization on anticancer mechanisms, Chem. A Eur. J. 22 (2016) 7800–7809, https://doi.org/10.1002/chem.201505160.
[54] A.M. El-Agrody, A.M. Fouda, E.S.A.E.H. Khattab, Halogenated 2-amino-4H-benzo [h]chromene derivatives as antitumor agents and the relationship between lipophilicity and antitumor activity, Med. Chem. Res. 26 (2017) 691–700, https://doi.org/10.1007/s00044-016-1773-x.
[55] J. Zhao, S. Zhi, H. Yu, R. Mao, J. Hu, W. Song, J. Zhang, Mitochondrial and nuclear DNA dual damage induced by 2-(2′-quinolyl)benzimidazole copper complexes with potential anticancer activity, RSC Ad. 7 (2017) 51162–51174, https://doi.org/10.1039/c7ra09102h.
[56] V. Thamilarasan, N. Sengottuvelan, N. Stalin, P. Srinivasan, G. Chakkaravarthi, Synthesis, interactions, molecular structure, biological properties and molecular docking studies on Mn, Co, Zn complexes containing acetylacetone and pyridine ligands with DNA duplex, J. Photochem. Photobiol. B Biol. 160 (2016) 110–120, https://doi.org/10.1016/j.jphotobiol.2016.03.018.